ACS Catalysis

Research Article

pubs.acs.org/acscatalysis

Nanometer-Sized MoS_2 Clusters on Graphene Flakes for Catalytic Formic Acid Decomposition

Victor O. Koroteev,[†,‡] Dmitri A. Bulushev,*[,§,⊥] Andrey L. Chuvilin,[∇,∥] Alexander V. Okotrub,[†,‡] and Lyubov G. Bulusheva[†,‡]

[†]Nikolaev Institute of Inorganic Chemistry, SB RAS, 3 Acad. Lavrentiev ave., 630090 Novosibirsk, Russia

[‡]Novosibirsk State University, 2 Pirogov str., 630090 Novosibirsk, Russia

[§]Chemical & Environmental Sciences Department, University of Limerick, Limerick, Ireland

[⊥]Boreskov Institute of Catalysis, SB RAS, 5 Acad. Lavrentiev ave., 630090 Novosibirsk, Russia

[∇]CIC nanoGUNE Consolider, E-20018 San Sebastian, Spain

[∥]IKERBASQUE, Basque Foundation for Science, Bilbao, Spain

Supporting Information

ABSTRACT: MoS_2 was deposited on graphene flakes via decomposition of MoS_3 in vacuum at different temperatures (500−800 °C). The materials obtained were tested for catalytic formic acid decomposition, giving mainly hydrogen and carbon dioxide. According to atom-resolved transmission electron microscopy study, a considerable amount of MoS_2 clusters with a mean size of 1 nm was formed on the graphene surface at 500 °C. Simulation of the structure of a cluster revealed the presence of Mo-edge atoms. Raising the preparation temperature up to 800 °C led to agglomeration of MoS_2 clusters and formation of thin crystalline MoS_2 particles 20−30 nm in size. The sample enriched with the MoS_2 clusters showed 6 times higher catalytic activity at 160 °C than the sample with the crystalline MoS_2 particles. This demonstrates that the observed nanometer-sized MoS_2 clusters are responsible for catalysis.

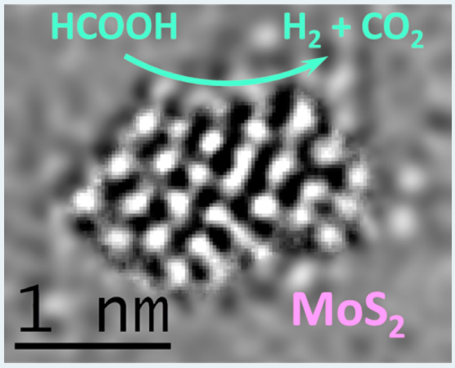

KEYWORDS: *MoS_2 clusters, graphene, structure, formic acid decomposition, hydrogen production*

1. INTRODUCTION

Two-dimensional (2D) materials, layered heterostructures, and low-dimensional hybrids have been attracting increased attention over the past few years. Among them is molybdenum disulfide (MoS_2), where metal atoms in a layer are sandwiched between two sheets of sulfur atoms.[1] MoS_2 monolayers have been isolated in a solution[2] after graphene,[3] but became a real fashion after the discovery of the scotch-tape method for exfoliating of layered materials[4] and the following decision of the Nobel Prize Committee.[5] At present, a variety of synthetic techniques are employed to form fullerene-like, nanotube, needle-like, monolayer, and flower-like MoS_2 structures.[6−11]

It is interesting that the structure of the active site in the natural nitrogenase-enzyme for the hydrogen evolution reaction (HER) is similar to the structure of the edge site of MoS_2.[12,13] In addition, theoretical and experimental studies show that conductivity, magnetism, and catalytic activity of nanostructured MoS_2 are often provided by edge sites, while basal atoms do not contribute substantially to these properties.[14−17] However, the edges in flat MoS_2 are not fully coordinated and, thus are energetically unstable, which makes formation of closed-shell structures thermodynamically preferable.[18−20] Moreover, MoS_2 may exist in different polymorphic forms distinguished by the layer arrangement and electronic properties.[21] Thus, recent studies showed that, compared to the hexagonal MoS_2, the trigonal polytype has a significantly enhanced electrocatalytic activity in HER,[22] and readily forms intercalates with lithium.[23] A high amount of edge atoms is expected for small-sized clusters, and although many research groups are focusing on the development of their synthesis,[24−30] the formation of clusters of <2 nm is still challenging due to their extremely high surface energy. A promising way to stabilize the edge MoS_2 atoms could be a growth of nanoparticles on a graphitic substrate.[12,24−30] It has been shown that graphene can promote the growth of hexagonal MoS_2 layers, although there is a lattice mismatch between these structures.[28]

In this work, we demonstrate that MoS_2 nanoclusters with an average size of 1 nm can be formed on a surface of graphene flakes via decomposition of MoS_3 at 500−600 °C. Further increase in the temperature causes growth of well-crystallized few-layer MoS_2 nanoparticles. Testing of MoS_2/graphene samples in the reaction of formic acid (HCOOH) decomposition demonstrates an important role of the 1-nm-sized

Received: July 2, 2014
Revised: September 10, 2014
Published: September 26, 2014

   dx.doi.org/10.1021/cs500943b | ACS Catal. 2014, 4, 3950−3956

MoS_2 clusters for catalytic activity. We are not aware of any studies of this reaction on MoS_2-based catalysts performed so far. However, hydrogen production from formic acid decomposition was widely studied recently in the framework of the green energy concept: this acid can be produced in a high concentration as a byproduct of the hydrolysis of cellulose from biomass,[31] and it can be used for hydrogen storage[32] and for catalytic hydrogenation or hydrodeoxygenation reactions as a hydrogen donor instead of molecular hydrogen.[33] Until now, mostly noble metal catalysts are studied for the decomposition while it is well-known that MoS_2 can participate in the same type of reactions.[34,35] A benefit of MoS_2 is that molybdenum is less-expensive and several orders of magnitude more abundant than noble metals;[36] in addition, MoS_2-based catalysts are tolerant to sulfur impurities, which are critical for certain applications.

2. EXPERIMENTAL SECTION

Graphene flakes were obtained by thermal exfoliation of graphite intercalated with nitric and sulfuric acids. The Brunauer–Emmett–Teller (BET) surface area and the total pore volume of the flakes were determined by N_2 adsorption after outgassing of the sample at 200 °C for 12 h using an Autosorb iQ Station. They were equal to 59 $m^2\ g^{-1}$ and 0.074 $cm^3\ g^{-1}$, respectively. The obtained relatively low surface area is typical for graphene materials prepared via the same method,[37,38] which gives stacks of graphene sheets with various thicknesses. MoS_2/graphene composites were synthesized by impregnation of the graphene flakes with a Mo-containing compound, followed by thermal decomposition, as described below. The flakes (100 mg) were suspended in 20 mL of a water–ethanol (1:1) solution with ammonium thiomolybdate $(NH_4)_2MoS_4$ (100 mg). The thiomolybdate was decomposed through the addition of concentrated HCl (0.5 mL), then the solution was filtered through a membrane and the obtained MoS_3/graphene sediment was washed by distilled water and dried in air. To convert MoS_3 to MoS_2, the samples were heated in vacuum (10^{-5} Pa) at 500, 600, 700, and 800 °C for 1 h. The content of Mo in the samples was expected to be equal to the surface Mo content (9 ± 3 wt %), as determined by X-ray photoelectron spectroscopy (XPS) for six samples. A 1 wt % Pt/C catalyst (Sigma–Aldrich) with a BET surface area of 650 $m^2\ g^{-1}$ studied earlier[39] was used for comparison of the catalytic activity.

The structure and composition of the samples were analyzed using high-resolution transmission electron microscopy (HR TEM), XPS, near-edge X-ray absorption fine structure (NEXAFS) and Raman scattering. TEM samples were prepared by ultrasound-assisted deposition of isopropanol suspension of the material on lacey carbon film grids. The measurements were done on a Titan 60-300 TEM/STEM microscope (FEI, Eindhoven, The Netherlands) at an acceleration voltage of 80 kV. Simulation of HR TEM images was made by MUSLI code,[40] utilizing atomistic models partially optimized by MM+ potential. NEXAFS and XPS experiments were performed at the Berliner Elektronenspeicherring für Synchrotronstrahlung (BESSY), using radiation from the Russian–German beamline. NEXAFS spectra near the C K-edge were acquired in the Auger-electron yield mode. The electrons emitted normal to the sample surface were measured, and the angle between the incident radiation and analyzer was 55°. The energy calibration was performed relatively to the π^*-band in graphite (285.4 eV). The energy resolution in the region of the C K-edge was 0.25 eV (full width at half-maximum, fwhm). The overall XPS spectrum, as well as the C 1s, S 2p, and Mo 3d lines, were measured using monochromatized radiation at 800 eV with an energy resolution of better than 0.4 eV (fwhm). In the spectrum analysis, the background signal was subtracted by Shirley's method. Raman spectra were acquired using a Triplemate 1877 spectrometer (Spex, Germany) with a 488-nm Ar^+ laser.

Catalytic experiments were performed as described earlier.[39,41,42] A quantity (0.024 g) of a MoS_2/graphene sample was placed in a quartz fixed-bed reactor with an internal diameter of 4 mm. All samples were pretreated in a 2 vol % H_2/He mixture at 350 °C for 1 h and cooled in He to the reaction temperature (100 °C). The reaction mixture contained 1.8 vol % of formic acid in He. All experiments were performed with a total flow rate of 51 cm^3 (STP) min^{-1}. The reactants and products were analyzed by a gas chromatography (GC) system (Agilent, Model HP-5890) fitted with a Porapak-Q column and a thermal conductivity detector.

3. RESULTS AND DISCUSSION

3.1. Electron Microscopy. Low-magnification TEM images show thin graphene flakes covered by dark nanoparticles with broad size distributions (see Figures 1a and 1b). These

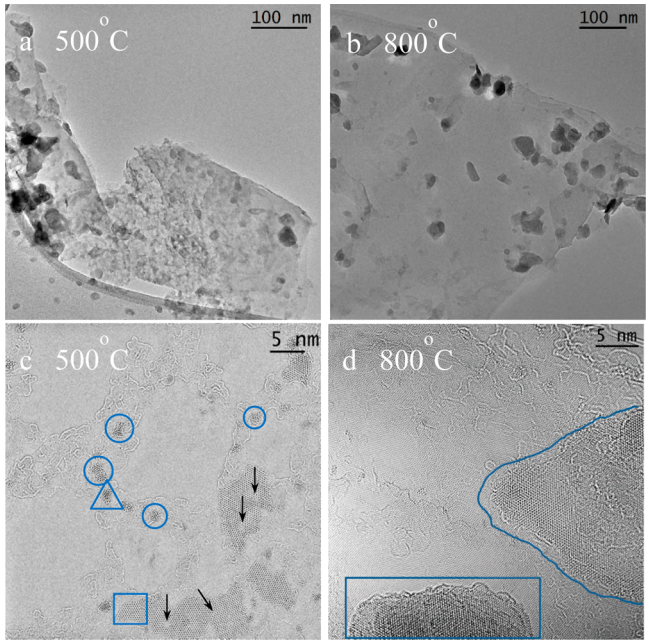

Figure 1. (a,b) Low-magnification and (c,d) high-magnification transmission electron microscopy (TEM) images of the MoS_2/graphene samples prepared at 500 °C (panels a and c) and 800 °C (panels b and d). Some of the MoS_2 clusters are shown by circle and triangle symbols in panel c and a part of a monolayer nanoisland is framed by a square. The arrows indicate holes and dislocations in nanoislands. Few-layer MoS_2 nanoparticles formed on the graphene surface are outlined in panel d.

nanoparticles were attributed to MoS_2, because the electron beam interacts more effectively with molybdenum and sulfur than with lighter carbon atoms. Comparing the images of the samples obtained at the lowest temperature (500 °C) (Figure 1a) and the highest temperature (800 °C) (Figure 1b), we conclude that the size of MoS_2 nanoparticles does not exceed 30 nm in both cases. Most of the nanoparticles recognized at

dx.doi.org/10.1021/cs500943b | ACS Catal. 2014, 4, 3950–3956

this magnification are ~10−20 nm in size. However, HRTEM analysis of the material obtained at 500 °C reveals hexagonal MoS_2 nanoislands and poorly crystallized molybdenum sulfide clusters (see Figure 1c). The nanoislands are monolayered and bilayered with an irregular shape. The presence of holes and dislocations (shown by arrows in Figure 1c) in the hexagonal lattice of MoS_2 implies coalescence of smaller crystallites during the synthesis. The basal plane size of nanoislands is often <10 nm, while the clusters consist of several Mo−S units. As the synthesis temperature increases, the amount of small clusters decreases significantly and monolayer nanoislands transform to thin nanoparticles 10−20 nm in size (see Figure 1d, marked with frames). The size distribution of clusters in the MoS_2/graphene hybrid synthesized at 500 °C was determined from statistical treatment of the HRTEM image presented in Figure 2a. One can see that the graphene surface is densely populated

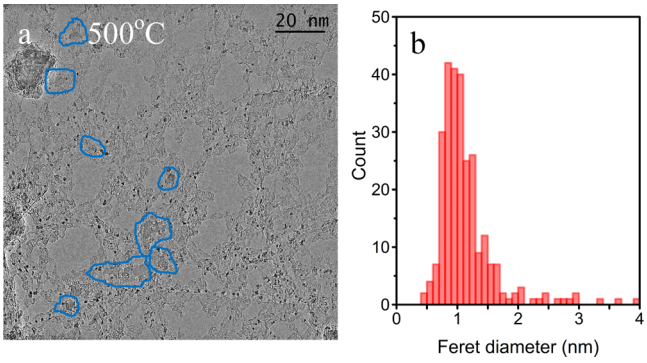

Figure 2. (a) High-resolution transmission electron microscopy (HRTEM) image of the MoS_2/graphene sample prepared at 500 °C and (b) size distribution of MoS_2 clusters. Some of MoS_2 nanoislands are outlined in panel a.

by black spots corresponding to the MoS_2 clusters, although the MoS_2 nanoislands (some of them are framed in Figure 2a) are also present. A histogram of the Feret diameters shows that the size of the clusters is mainly in the range of 0.6−1.7 nm, with the mean value of ~1 nm (see Figure 2b).

In order to recognize the structure of clusters and nanoislands, we analyzed the HRTEM images of the areas framed by the triangle and square symbols in Figure 1c. The enlarged images are presented in Figures 3a and 4a,

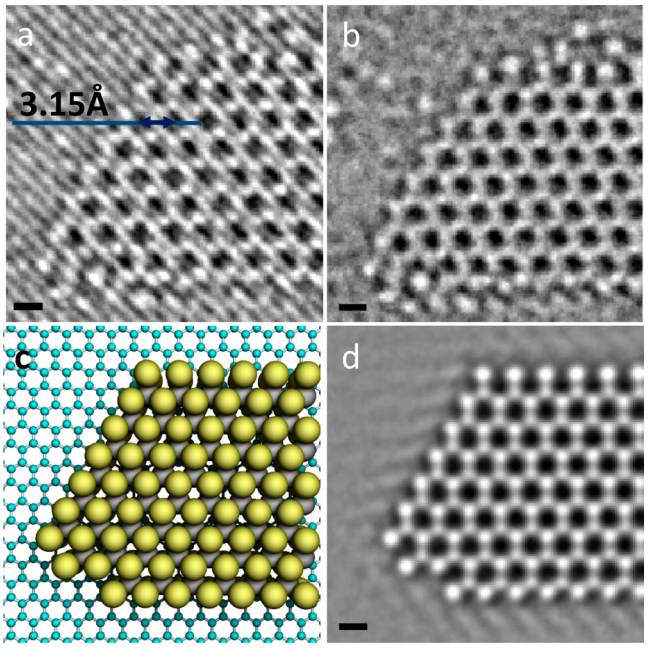

Figure 4. (a) HRTEM and (b) FFT-filtered HRTEM images of a fragment of a monolayer MoS_2 nanoisland. The image is the enlarged fragment taken from Figure 1c (shown by the square symbol). Simulated image for the model of hexagonal MoS_2 monolayer (panel d) with corresponding atomic structure (panel c), where Mo atoms and S atoms are gray and yellow, respectively. The scale mark is 5 Å.

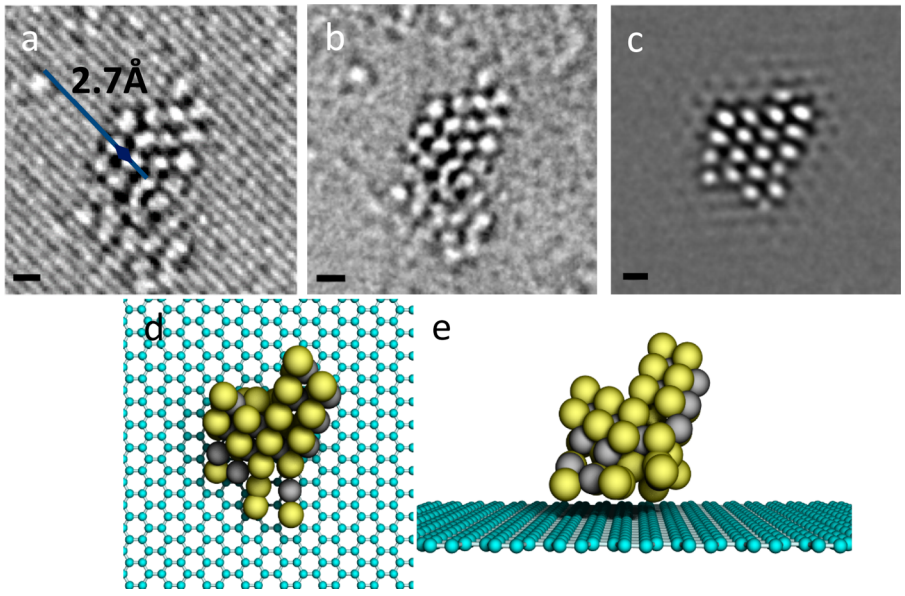

Figure 3. (a) HRTEM and (b) fast Fourier transform (FFT)-filtered HRTEM image of a MoS_2 cluster. The image is enlarged fragment taken from Figure 1c (shown by triangle). (c) Simulated image for the model of the MoS_2 cluster with corresponding atomic structure ((d) top view and (e) side view), where Mo atoms and S atoms are gray and yellow, respectively. The scale mark is 5 Å.

dx.doi.org/10.1021/cs500943b | ACS Catal. 2014, 4, 3950−3956

respectively. Although atoms in the cluster are hexagonally arranged, the in-plane distance between bright spots is ~2.7 Å (Figure 3a). This means that some MoS_2 layers are not aligned with the graphene surface and could be laying on the edge.

The nanoisland is represented by a honeycomb MoS_2 monolayer with a distance of 3.15 Å between the centers of hexagons (Figure 4a). According to Bollinger et al.,[43] Mo atoms on the $(10\bar{1}0)$ edge (called the Mo-edge) without sulfur coverage are thermodynamically unstable and the edge is reconstructed, making Mo atoms fully coordinated with sulfur. The $(\bar{1}010)$ edge (called S-edge) is stable, but when S vacancies are present, the under-coordinated Mo atoms may exist on this edge. Recently, Zhou et al.[44] observed the Mo-terminated edges without sulfur coverage in MoS_2 monolayers formed in Mo-rich or S-deficient growth conditions.

To clarify the atomic positions and exclude underlying graphene lattice, we filtered the images using fast Fourier transform (FFT). The obtained images of the cluster and monolayer are presented in Figures 3b and 4b, respectively. FFT TEM images of three other clusters are shown in Figure S1 in the Supporting Information. They all have a typical distance between the spots of ~2.7 Å. To make a model of the molybdenum suflide cluster, we considered MoS_2 fragments laying inclined on the surface of graphene. The HRTEM image of the model is presented in Figure 3c. The cluster consists of fragments of hexagonal MoS_2 layers, which are inclined relative to the graphene plane at an angle, providing a separation distance of 2.7 Å in the top-view projection on the graphene plane (Figure 3d). A side-view projection (Figure 3e) clearly shows this. The composition of the model is close to MoS_2 and it has a Mo vacancy and some under-coordinated Mo atoms on the edges. The fact that small MoS_2 clusters may be not laying parallel to the graphene plane is quite interesting itself, since, with a decrease of the size, the mean surface energy increases and a contribution from the cluster alignment could be significant. Recently, Walton et al.[45] have shown that the shapes of the MoS_2 nanoparticles and clusters are dependent on the support material. Thus, MoS_2 nanoparticles forming on the gold surface are mostly trigonal, while those deposited on highly ordered pyrolitic graphite have a hexagonal or round shape. In our case, the formation of MoS_2 starts from clusters, where some layers are not parallel to the substrate, which is not a trivial result. To simulate the HRTEM image of the MoS_2 monolayer fragment, we constructed a model where the Mo-edges have 100% S-coverage (see Figures 4c and 4d). Such coverage is due to sulfur excess in our synthesis. In the case of 50% S-coverage, we would see a shift of the last row by 1/2 period, because of the edge reconstruction.[43]

3.2. Spectroscopy. It could be expected that molybdenum carbide (Mo_2C) is formed on the interface between the MoS_2 clusters and the graphene surface. It is quite difficult to detect small amounts of these species reliably. NEXAFS C K-edge spectroscopy is considered as the most promising technique for this purpose, as Mo_2C provides a sharp intense resonance at 288.5 eV.[46] In the spectra of our samples, this resonance was absent independent of the synthesis temperature (see Figure S2 in the Supporting Information). The observed spectra reflect only the graphene support. In accordance, no formation of Mo_2C was reported for different MoS_2/C systems in the literature.[28,45] Therefore, we support the van der Waals interaction model for the growth of a MoS_2 cluster on a graphene surface proposed by Shi et al.[28] This is also in agreement with the data that graphene-based materials interact with MoS_2 only weakly as compared to oxide supports.[45,47] Such a weak interaction may provide an improved catalytic activity of MoS_2 species.

We analyzed the chemical state of molybdenum and sulfur using the sample obtained at 600 °C as an example. The surface concentrations of molybdenum, sulfur, and oxygen determined from the survey XPS spectrum are 1.5, 2.7, and 4.3 at. %, respectively. The high-resolution XPS S 2p spectrum was fitted with three $2p_{3/2}$–$2p_{1/2}$ spin–orbit doublets separated by ~1.2 eV with the intensity ratio of 2:1 (see Figure 5a). The $2p_{3/2}$

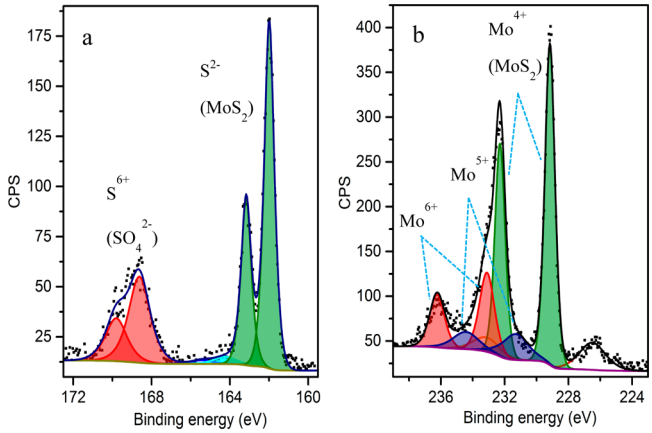

Figure 5. X-ray photoelectron spectroscopy (XPS) spectra of (a) S 2p and (b) Mo 3d regions for the MoS_2/graphene sample prepared at 600 °C.

component of the main doublet is located at a binding energy of ~162.0 eV, which is characteristic for sulfide ions (S^{2-}).[48,49] The $2p_{3/2}$ component at 168.6 eV is assigned to the S^{6+} state realized in SO_4^{2-} groups.[50] Since after the synthesis the soluble salts were washed away of the sample, these groups could be located at the edges of MoS_2 nanoparticles. A weak doublet with S $2p_{3/2}$ energy of 164.2 eV could be assigned to disulfides (S_2^{2-}) formed at the MoS_2 edges or elemental sulfur.[51]

The X-ray photoelectron spectroscopy (XPS) spectrum in the Mo 3d energy region was fitted with eight components (Figure 5b). The low-energy peak centered at 226.3 eV and the component at 233.2 eV are assigned to the binding energies of the 2s electrons of S^{2-} and S^{6+}, respectively. The remaining components originate from three Mo $3d_{5/2}$–$3d_{3/2}$ spin–orbit doublets separated by ~3.1 eV with the intensity ratio of 3:2. The energy of the doublet increases as the degree of Mo oxidation increases. The intense $3d_{5/2}$ component at ~229.1 eV corresponds to the Mo^{4+} state realized in MoS_2, the component with an energy of ~231.2 eV could be assigned to the Mo^{5+} state, and the low-energy $3d_{5/2}$ component at 233.1 eV is due to the Mo^{6+} contribution.[50,52] Notice that the XPS analysis was done for the sample after the reduction in a H_2/He flow at 350 °C for 1 h, followed by catalytic experiments. This treatment removes not only oxygen but also some sulfur,[34,53] resulting in a Mo:S ratio slightly higher than 1:2 for our sample. Literature data[34,53] for some MoS_2-based samples indicate slightly overstoichiometric S:Mo ratios, even after reduction with hydrogen at 400 °C. The lower ratio (1.8) in our case is probably related to the presence of MoS_2 nanoclusters with an excess of Mo-edge sites. The Mo^{5+} and Mo^{6+} species may be formed in the sample during storage at ambient conditions. This is in agreement with literature data.[34,50,54,55] A relatively

dx.doi.org/10.1021/cs500943b | ACS Catal. 2014, 4, 3950–3956

high content of such species in our samples indicates the presence of a high concentration of Mo-edge sites.

Raman spectra of the MoS_2/graphene samples exhibit three main peaks in the range of 300−1800 cm^{-1} (see Figure 6). The

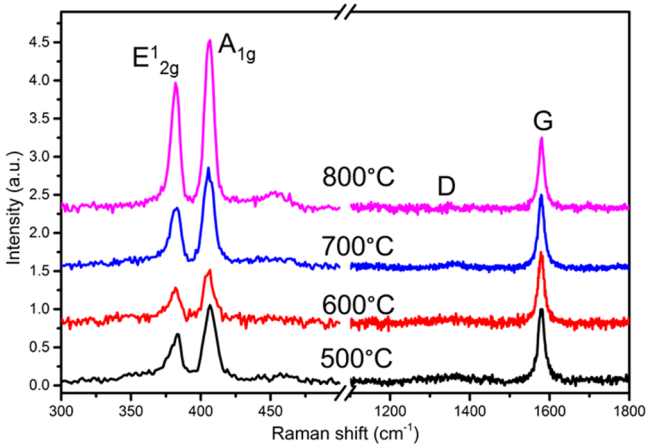

Figure 6. Raman spectra of the MoS_2/graphene samples prepared at different temperatures.

peak located at ~1579 cm^{-1} corresponds to C−C bond stretching in the graphene plane (G-band). All the spectra have a negligible intensity of the scattering induced by disorder in the graphitic lattice (D-band), indicating high atomic ordering of the substrate. Displacements of atoms in the hexagonal MoS_2 layer contribute to the peaks located at ~382 and ~406 cm^{-1} and are assigned to the E^1_{2g} and A_{1g} vibration modes.[6,56,57] The peaks are only slightly shifted as the temperature of the MoS_2/graphene synthesis increases, while their broadness progressively decreases. This behavior is due to the increase of MoS_2 particle sizes and crystallinity with the rise of the synthesis temperature from 500 °C to 800 °C. Comparing the spectra normalized to the intensity of graphitic G-band, one can see that the amount of crystalline MoS_2 for the samples obtained at 500 and 600 °C is almost the same and further increases in temperature result in the observed increase of the MoS_2 peaks intensity provided by the increasing amount of MoS_2 crystal nanoparticles. These data are in accordance with the TEM observations (see Figures 1c and 1d), demonstrating the disappearance of the MoS_2 clusters and the growth of bigger hexagonal particles with temperature.

3.3. Catalysis. The MoS_2/graphene samples obtained at different temperatures were studied in catalytic decomposition of formic acid vapor (Figure 7). The formic acid decomposition is seen at ~100 °C for the samples synthesized at 500 and 600 °C and reaches 100% conversion at ~250 °C (see Figure 7a). As the synthesis temperature increases from 500 °C to 800 °C, the conversion curve shifts by ~30 °C to higher temperatures and the reaction rate decreases by a factor of 6 at 160 °C (see Figure 7b). Activation energies were calculated for the formic acid decomposition from the Arrhenius plots (see Figure S3 in the Supporting Information). They were equal to 81 ± 4 kJ mol^{-1}, being independent of the synthesis temperature. This clearly indicates that the observed difference in the catalytic activity is related to a change of the concentration of active sites, but not to a change of the activation energy. This result is consistent with the Raman scattering measurements (Figure 6), showing aggregation of MoS_2 with temperature, and indicates that the MoS_2 clusters ~1 nm in size observed by TEM (Figure 2b, 3) are the major active catalytic species.

The products of formic acid decomposition are mostly composed by CO_2, hydrogen, and methyl formate (Figure 8).

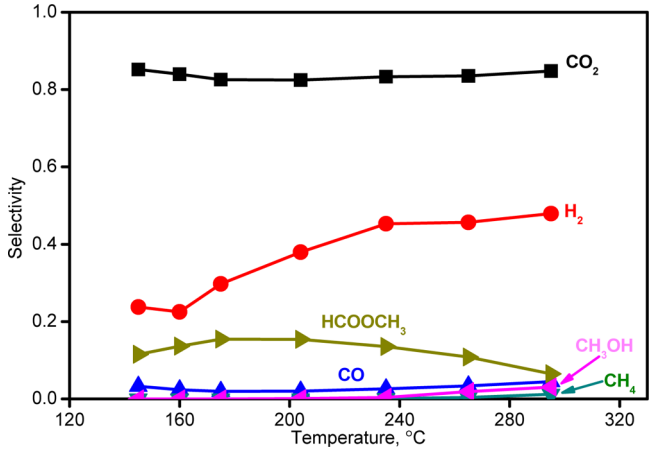

Figure 8. Selectivity to different products at different temperatures for the MoS_2/graphene catalyst prepared at 500 °C.

Water vapor was not controlled in our study, but it must be formed according to a hydrogen balance. CO_2 and hydrogen are typical products of formic acid dehydrogenation on noble metal catalysts.[32,39,41,42] It is seen that the hydrogen selectivity

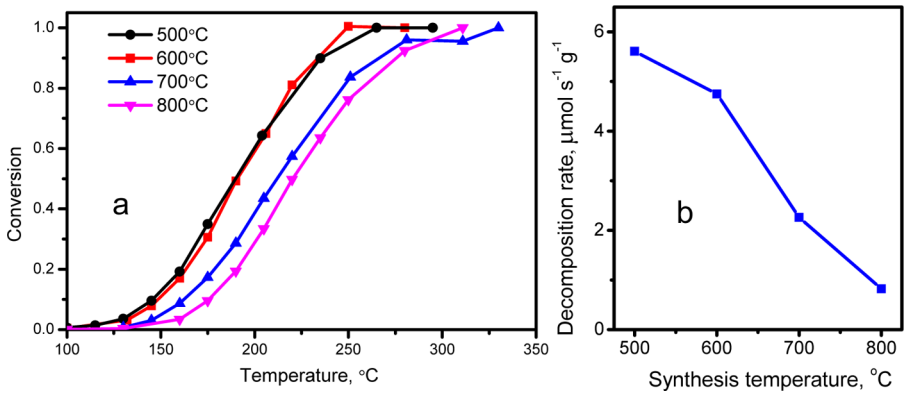

Figure 7. (a) Steady-state conversions of formic acid versus temperature for the MoS_2/graphene catalysts prepared at different temperatures and (b) rates of the formic acid decomposition at 160 °C as a function of the synthesis temperature.

dx.doi.org/10.1021/cs500943b | ACS Catal. 2014, 4, 3950−3956

Table 1. Effect of Water Vapor (2.5 vol %) on the Conversion and Selectivity of Product Formation for the Formic Acid Decomposition at 235°C on the MoS_2/Graphene Catalyst Prepared at 500 °C

		Selectivity					
	conversion	H_2	CO_2	CO	methyl formate	methanol	CH_4
without H_2O	0.920	0.42	0.83	0.026	0.121	0.017	0.003
with H_2O	0.863	0.49	0.89	0.020	0.048	0.043	0.002

increases with temperature/conversion, while the selectivity to CO_2 almost does not change. The formation of methyl formate indicates that hydrogen produced from formic acid may reduce this acid to methanol or methoxy species, which can further interact with formic acid, giving the ester. Consequently, at higher temperatures, traces of methanol and methane are observed. It is also seen that the selectivity curve of the methyl formate formation, as a function of temperature, passes through a maximum. At high temperatures, this ester can be hydrolyzed by water vapor present in the products, giving methanol and formic acid. This was confirmed by experiments with the addition of water vapor to the reaction mixture containing formic acid (see Table 1). The addition led to a decrease in the methyl formate selectivity and an increase in the methanol selectivity. The selectivities to the other products, as well as the conversion, did not change noticeably in the presence of water. When the decomposition temperature reaches 200 °C, traces of CO are observed. This product can be formed as a result of the dehydration of formic acid or the reverse water−gas shift reaction. We have not observed any reaction of CO with hydrogen (0.5 vol % CO, 1.6 vol % H_2 in He) on the samples studied at temperatures up to 450 °C. Thus, neither of the products observed is a result of the hydrogenation of CO.

Recently, Koos and Solymosi[58] studied the decomposition of formic acid over Mo_2C catalysts supported on different forms of carbon under conditions similar to ours. Since they worked at the same range of temperatures, the activities of carbides and sulfides are close. This probably also indicates similar active sites for the decomposition reaction. Koos and Solymosi supposed that carbon-deficient sites of Mo_2C could be important for the formic acid decomposition taking place via the formation/decomposition of formate species. The formate route was confirmed later by density functional theory calculations of Luo et al.[59] These considerations also could be important for MoS_2 catalysts. As compared to the MoS_2 catalysts, the Mo_2C catalysts gave higher hydrogen selectivity (95−100%) and provided no formation of methyl formate and methanol. However, it should be taken into account that further improvement of the properties of the MoS_2 catalysts by doping seems possible and using of Mo_2C as a catalyst is complicated, since this material is highly pyrophoric.

We also compared the activity related to the molybdenum content for the best MoS_2/graphene catalyst with the activity related to the platinum content for the Pt catalyst supported on activated carbon at 145 °C (see Table S1 in the Supporting Information). The mean size of Pt clusters was equal to 1.6 nm,[39] which was quite similar to the size of MoS_2 clusters. The activity of Pt was 7 times higher. However, it should be taken into account that the price of molybdenum is considerably lower than that of platinum.

4. CONCLUSIONS

We have shown a principal possibility to synthesize nanometer-sized MoS_2 clusters on the graphene surface. Decreasing the decomposition temperature in the synthesis to 500 °C has led to a high concentration of 1-nm-sized MoS_2 clusters in the material. At higher temperatures, the aggregation of the clusters into well-crystallized islands 20−30 nm in size has been observed. The increase in the size of MoS_2 particles and their crystallinity correlate with the decrease of the catalytic activity of the MoS_2/graphene material in the decomposition of formic acid. This correlation allows one to suggest that this reaction occurs on the Mo-edge atoms exposed mainly by the MoS_2 clusters. Optimization of the synthetic procedure aiming to a MoS_2/graphene catalyst containing solely 1-nm-sized clusters may lead to highly active catalysts for different important reactions taking place on MoS_2 edge sites, such as hydrogen evolution reaction or hydroprocessing of petroleum fractions. It is also important that formic acid could be used not only as a probe to test active sites of MoS_2 catalysts, but also as a hydrogen donor for reactions involving hydrogen and these catalysts.

■ ASSOCIATED CONTENT

Supporting Information

Comparison of the catalytic activity of MoS_2/graphene and Pt/C catalysts (Table S1), HRTEM images of MoS_2 clusters (Figure S1), C K-edge NEXAFS spectra (Figure S2), and Arrhenius plots (Figure S3). This material is available free of charge via the Internet at http://pubs.acs.org.

■ AUTHOR INFORMATION

Corresponding Author

*E-mail: dmitri.bulushev@ul.ie.

Notes

The authors declare no competing financial interest.

■ ACKNOWLEDGMENTS

The synthetic part of the work was done with the financial support of the Russian Foundation for Basic Research (Grant No. 14-03-31633). This publication has also emanated from research conducted with the financial support of Science Foundation Ireland (under Grant No. 06/CP/E007). Collaboration between partner institutions was partly supported by Grant No. FP7-PEOPLE-2011-IRSES N295180 (MagNonMag).

■ REFERENCES

(1) Johari, P.; Shenoy, V. B. *ACS Nano* **2011**, *5*, 5903−5908.
(2) Joensen, P.; Frindt, R. F.; Morrison, S. R. *Mater. Res. Bull.* **1986**, *21*, 457−461.
(3) Boehm, H. P.; Clauss, A.; Fischer, G. O.; Hofmann, U. *Z. Anorg. Allg. Chem.* **1962**, *316*, 119−127.
(4) Novoselov, K. S.; Geim, A. K.; Morozov, S. V.; Jiang, D.; Zhang, Y.; Dubonos, S. V.; Grigorieva, I. V.; Firsov, A. A. *Science* **2004**, *306*, 666−669.
(5) *Nobel Prizes in Physics 2010*. http://www.nobelprize.org/nobel_prizes/physics/laureates/2010, accessed October 5, 2014.
(6) Afanasiev, P. *C. R. Chim.* **2008**, *11*, 159−182.

(7) Albu-Yaron, A.; Levy, M.; Tenne, R.; Popovitz-Biro, R.; Weidenbach, M.; Bar-Sadan, M.; Houben, L.; Enyashin, A. N.; Seifert, G.; Feuermann, D.; Katz, E. A.; Gordon, J. M. *Angew. Chem.—Int. Ed.* **2011**, *50*, 1810−1814.
(8) Koroteev, V. O.; Bulusheva, L. G.; Okotrub, A. V.; Yudanov, N. F.; Vyalikh, D. V. *Phys. Status Solidi B* **2011**, *248*, 2740−2743.
(9) Leist, A.; Stauf, S.; Loken, S.; Finckh, E. W.; Ludtke, S.; Unger, K. K.; Assenmacher, W.; Mader, W.; Tremel, W. *J. Mater. Chem.* **1998**, *8*, 241−244.
(10) Ma, L.; Chen, W. X.; Li, H.; Xu, Z. D. *Mater. Chem. Phys.* **2009**, *116*, 400−405.
(11) Bar-Sadan, M.; Enyashin, A. N.; Gemming, S.; Popovitz-Biro, R.; Hong, S. Y.; Prior, Y.; Tenne, R.; Seifert, G. *J. Phys. Chem. B* **2006**, *110*, 25399−25410.
(12) Fukuzumi, S. *Eur. J. Inorg. Chem.* **2008**, 1351−1362.
(13) Hinnemann, B.; Moses, P. G.; Bonde, J.; Jorgensen, K. P.; Nielsen, J. H.; Horch, S.; Chorkendorff, I.; Norskov, J. K. *J. Am. Chem. Soc.* **2005**, *127*, 5308−5309.
(14) Kibsgaard, J.; Chen, Z. B.; Reinecke, B. N.; Jaramillo, T. F. *Nat. Mater.* **2012**, *11*, 963−969.
(15) Kong, D. S.; Wang, H. T.; Cha, J. J.; Pasta, M.; Koski, K. J.; Yao, J.; Cui, Y. *Nano Lett.* **2013**, *13*, 1341−1347.
(16) Lauritsen, J. V.; Kibsgaard, J.; Helveg, S.; Topsoe, H.; Clausen, B. S.; Laegsgaard, E.; Besenbacher, F. *Nat. Nanotechnol.* **2007**, *2*, 53−58.
(17) Shidpour, R.; Manteghian, M. *Chem. Phys.* **2009**, *360*, 97−105.
(18) Bar Sadan, M.; Houben, L.; Enyashin, A. N.; Seifert, G.; Tenne, R. *Proc. Natl. Acad. Sci. U.S.A.* **2008**, *105*, 15643−15648.
(19) Deepak, F. L.; Mayoral, A.; Yacaman, M. J. *Appl. Phys. A: Mater. Sci. Process.* **2009**, *96*, 861−867.
(20) Hu, J. J.; Sanders, J. H.; Zabinski, J. S. *J. Mater. Res.* **2006**, *21*, 1033−1040.
(21) Wypych, F.; Sollmann, K.; Schollhorn, R. *Mater. Res. Bull.* **1992**, *27*, 545−553.
(22) Lukowski, M. A.; Daniel, A. S.; Meng, F.; Forticaux, A.; Li, L. S.; Jin, S. *J. Am. Chem. Soc.* **2013**, *135*, 10274−10277.
(23) Stephenson, T.; Li, Z.; Olsen, B.; Mitlin, D. *Energy Environ. Sci.* **2014**, *7*, 209−231.
(24) Klimenko, I. V.; Golub, A. S.; Zhuravleva, T. S.; Lenenko, N. D.; Novikov, Y. N. *Russ. J. Phys. Chem. A* **2009**, *83*, 276−280.
(25) Koroteev, V. O.; Bulusheva, L. G.; Okotrub, A. V.; Yushina, I. V. *J. Nanoelectr. Optoelectr.* **2012**, *7*, 50−53.
(26) Lauritsen, J. V.; Nyberg, M.; Vang, R. T.; Bollinger, M. V.; Clausen, B. S.; Topsoe, H.; Jacobsen, K. W.; Laegsgaard, E.; Norskov, J. K.; Besenbacher, F. *Nanotechnology* **2003**, *14*, 385−389.
(27) Remskar, M.; Mrzel, A.; Skraba, Z.; Jesih, A.; Ceh, M.; Demsar, J.; Stadelmann, P.; Levy, F.; Mihailovic, D. *Science* **2001**, *292*, 479−481.
(28) Shi, Y. M.; Zhou, W.; Lu, A. Y.; Fang, W. J.; Lee, Y. H.; Hsu, A. L.; Kim, S. M.; Kim, K. K.; Yang, H. Y.; Li, L. J.; Idrobo, J. C.; Kong, J. *Nano Lett.* **2012**, *12*, 2784−2791.
(29) Wilcoxon, J. P.; Newcomer, P. P.; Samara, G. A. *J. Appl. Phys.* **1997**, *81*, 7934−7944.
(30) Zak, A.; Feldman, Y.; Alperovich, V.; Rosentsveig, R.; Tenne, R. *J. Am. Chem. Soc.* **2000**, *122*, 11108−11116.
(31) Girisuta, B.; Dussan, K.; Haverty, D.; Leahy, J. J.; Hayes, M. H. B. *Chem. Eng. J.* **2013**, *217*, 61−70.
(32) Grasemann, M.; Laurenczy, G. *Energy Environ. Sci.* **2012**, *5*, 8171−8181.
(33) Bulushev, D. A.; Ross, J. R. H. *Catal. Today* **2011**, *163*, 42−46.
(34) Duchet, J. C.; Vanoers, E. M.; Debeer, V. H. J.; Prins, R. *J. Catal.* **1983**, *80*, 386−402.
(35) Bremaud, M.; Vivier, L.; Perot, G.; Harle, V.; Bouchy, C. *Appl. Catal., A* **2005**, *289*, 44−50.
(36) Flaherty, D. W.; Berglund, S. P.; Mullins, C. B. *J. Catal.* **2010**, *269*, 33−43.
(37) Focke, W. W.; Badenhorst, H.; Mhike, W.; Kruger, H. J.; Lombaard, D. *Thermochim. Acta* **2014**, *584*, 8−16.
(38) Vieira, F.; Cisneros, I.; Rosa, N. G.; Trinidade, G. M.; Mohallem, N. D. S. *Carbon* **2006**, *44*, 2587−2592.
(39) Bulushev, D. A.; Jia, L. J.; Beloshapkin, S.; Ross, J. R. H. *Chem. Commun.* **2012**, *48*, 4184−4186.
(40) Chuvilin, A.; Kaiser, U. *Ultramicroscopy* **2005**, *104*, 73−82.
(41) Bulushev, D. A.; Beloshapkin, S.; Plyusnin, P. E.; Shubin, Y. V.; Bukhtiyarov, V. I.; Korenev, S. V.; Ross, J. R. H. *J. Catal.* **2013**, *299*, 171−180.
(42) Jia, L. J.; Bulushev, D. A.; Podyacheva, O. Y.; Boronin, A. I.; Kibis, L. S.; Gerasimov, E. Y.; Beloshapkin, S.; Seryak, I. A.; Ismagilov, Z. R.; Ross, J. R. H. *J. Catal.* **2013**, *307*, 94−102.
(43) Bollinger, M. V.; Jacobsen, K. W.; Norskov, J. K. *Phys. Rev. B* **2003**, *67*, 085410.
(44) Zhou, X. S.; Wan, L. J.; Guo, Y. G. *Chem. Commun.* **2013**, *49*, 1838−1840.
(45) Walton, A. S.; Lauritsen, J. V.; Topsoe, H.; Besenbacher, F. *J. Catal.* **2013**, *308*, 306−318.
(46) Berhault, G.; Mehta, A.; Pavel, A. C.; Yang, J. Z.; Rendon, L.; Yacaman, M. J.; Araiza, L. C.; M?ller, A. D.; Chianelli, R. R. *J. Catal.* **2001**, *198*, 9−19.
(47) Kibsgaard, J.; Clausen, B. S.; Topsoe, H.; Laegsgaard, E.; Lauritsen, J. V.; Besenbacher, F. *J. Catal.* **2009**, *263*, 98−103.
(48) Baker, M. A.; Gilmore, R.; Lenardi, C.; Gissler, W. *Appl. Surf. Sci.* **1999**, *150*, 255−262.
(49) Koroteev, V. O.; Okotrub, A. V.; Bulusheva, L. G. *Full. Nanotube Carbon Nanostruct.* **2011**, *19*, 39−43.
(50) Bonde, J.; Moses, P. G.; Jaramillo, T. F.; Norskov, J. K.; Chorkendorff, I. *Faraday Discuss.* **2008**, *140*, 219−231.
(51) Smart, R. S.; Skinner, W. M.; Gerson, A. R. *Surf. Interface Anal.* **1999**, *28*, 101−105.
(52) Fuchtbauer, H. G.; Tuxen, A. K.; Li, Z. S.; Topsoe, H.; Lauritsen, J. V.; Besenbacher, F. *Top. Catal.* **2014**, *57*, 207−214.
(53) Afanasiev, P. *J. Catal.* **2010**, *269*, 269−280.
(54) Chianelli, R. R.; Berthault, G.; Torres, B. *Catal. Today* **2009**, *147*, 275−286.
(55) Voiry, D.; Salehi, M.; Silva, R.; Fujita, T.; Chen, M.; Asefa, T.; Shenoy, V. B.; Eda, G.; Chhowalla, M. *Nano Lett.* **2013**, *13*, 6222−6227.
(56) Lee, C.; Yan, H.; Brus, L. E.; Heinz, T. F.; Hone, J.; Ryu, S. *ACS Nano* **2010**, *4*, 2695−2700.
(57) Li, S. L.; Miyazaki, H.; Song, H.; Kuramochi, H.; Nakaharai, S.; Tsukagoshi, K. *ACS Nano* **2012**, *6*, 7381−7388.
(58) Koos, A.; Solymosi, F. *Catal. Lett.* **2010**, *138*, 23−27.
(59) Luo, Q. Q.; Wang, T.; Walther, G.; Beller, M.; Jiao, H. J. *J. Power Sources* **2014**, *246*, 548−555.